



Carbohydrate Polymers

www.elsevier.com/locate/carbpol

Carbohydrate Polymers 72 (2008) 444-455

Biodegradability and property characterizations of Methyl Cellulose: Effect of nanocompositing and chemical crosslinking

Sarawut Rimdusit ^{a,*}, Sorada Jingjid ^a, Siriporn Damrongsakkul ^a, Sunan Tiptipakorn ^a, Tsutomu Takeichi ^b

^a Department of Chemical Engineering, Faculty of Engineering, Chulalongkorn University, Bangkok 10330, Thailand
^b School of Materials Science, Toyohashi University of Technology, Tempaku-cho, Toyohashi 441-8580, Japan

Received 1 August 2007; received in revised form 4 September 2007; accepted 11 September 2007 Available online 19 September 2007

Abstract

Broader range of biodegradability and other essential properties of Methyl Cellulose (MC) were achieved through nanocomposite formation and chemical crosslinking. Methyl Cellulose/Montmorillonite (MC/MMT) nanocomposites as well as MC-glutaraldehyde crosslinked films were characterized for thermal properties, tensile properties, moisture absorption, and biodegradability. MC/MMT nanocomposite films prepared by MMT suspension exhibited exfoliation which was confirmed by XRD and TEM results. In the chemical crosslinked system, the FTIR spectra revealed the crosslinkage between MC and GA. The tensile properties of the crosslinked films indicated that optimum GA content was 4.5 wt%. In addition, MC prepared from each method was capable of enhancing different properties. The MC/MMT nanocomposites could significantly improve tensile modulus (nanocompositing: 65%; crosslinking: 45%), while MC crosslinked film could outstandingly increase glass transition temperature (nanocompositing: 4 °C; crosslinking: 17 °C) and decrease moisture absorption properties (nanocompositing: 19%; crosslinking: 26%). The crosslinkage technique had more potential to hinder the biodegradation process. In 6 weeks, the CO₂ emission of crosslinked films was reduced around 80% in comparison with that of pure MC. © 2007 Elsevier Ltd. All rights reserved.

Keywords: Montmorillonite; Methyl Cellulose; Nanocomposite; Exfoliation; Biodegradability

1. Introduction

In the past 20 years, the production and the use of plastics in the world have been enormously increased, worsening the problems of the waste disposal. The growing interest in environmental impact of discarded plastics has been focused on the development of plastics, which are degraded more rapidly in the environment, leading to a complete bioassimilation of the plastics (Aminabhavi, Balundgi, & Cassidy, 1990; Crosby, 1981; Doi, 1990). Biopolymers can be used in those applications where biodegradability and/or the derivation of natural resources gives added value, particularly, where valuable petroleum-based plastics are used for applications with a short life

time (Avella et al., 2005). For these reasons, throughout the world today, the development of biodegradable materials with controlled properties has been a subject of great research challenge to the community of material scientists and engineers (Gupta & Revagade, 2007; Mangiacapra, Gorrasi, Sorrentino, & Vittoria, 2005; Marras, Zuburtikudis, & Panayiotou, 2007; Yang, Yu, Feng, & Ma, 2006).

Methyl Cellulose (MC), a biodegradable polymer, is a modified type of cellulose being the most abundant biopolymer in nature. It is well known and of interest to be used as environmental friendly products, especially as coating or mulching film, because of its large availability, low cost, and easy processability. However, due to a biodegradable behavior of MC, it can be used only in limited applications.

There are two methods that can be used to potentially improve the biodegradability of MC. The first method is

^{*} Corresponding author. Tel.: +662 218 6862; fax: +662 218 6877. E-mail address: sarawut.r@chula.ac.th (S. Rimdusit).

nanoreinforcement of pristine polymers to increase the lengths of the tortuous paths in nanocomposites in the presence of high clay content. When these lengths increase, the clay with high aspect ratio obstructs the diffusion of microorganism in the bulk of the film. That forces the decrease of biodegradability rate (Lee et al., 2002). The second one is to promote covalent linkages between polymer chains by crosslinking agent such as glutaraldehyde (GA). When crosslinkages occur, the gaps between polymer chains reduce. The water molecules, which are the media of microorganism, cannot penetrate through the crosslinked polymers. Both methods should modulate the biodegradability of polymers.

Polymer/clay nanocomposites have been the focus of academic and industrial attention in recent years because the final composites often exhibit a desired enhancement of physical and/or chemical properties relative to the pure polymer matrix e.g. increase of strength (Kampeerapappun, Aht-Ong, Pentrakoon, & Srikulkit, 2007), enhancement of thermal stability, and especially decrease of biodegradability rate even at very low clay contents (Lee et al., 2002; Li, Chen, & Xie, 2004; Wang et al., 2005). Montmorillonite (MMT) is one of the most important natural clays. The filler originally inherits a stacked structure of parallel silicate layers (Sinha & Okamoto, 2003). Depending on the extent of compatibility between the clay and the matrix, a microphase-separated conventional composite, intercalated, or exfoliated morphology can be obtained when directly mixed with polymer matrix (Krikorian & Pochan, 2003).

Crosslinking is one of the most popular methods used to modify water-soluble polymer in order to achieve desired properties. Some polymer characteristics could be altered by crosslinking such as swelling, permeability (Coma, Sebti, Pardon, Pichavant, & Deschamps, 2003; Park & Ruckenstein, 2001), drug releasing, transport properties, water uptake, mechanical properties, chemical stability, sponge structure as well as biodegradation rate (Wach, Mitomo, Nagasawa, & Yoshii, 2003). Several crosslinking agents for MC have been employed including dialdehyde. However, one of the most popular crosslinkers is glutaral-dehyde (GA), a small molecule dialdehyde (Park & Ruckenstein, 2001).

In this work, MC/MMT nanocomposite films were prepared by solution intercalation using a homogenizer at the MC gelatinized temperature of 50–55 °C, to achieve intercalation of the stacked layers of MMT. The filler was suspended in water and dispersed under ultra high shear rate to form MMT gel suspension. This preparation method was applied in order to delaminate the layered silicate of MMT and to homogenously disperse the nanoparticles in MC matrix. Crosslinked MC was prepared by using GA as a chemical crosslinking reagent and hydrochloric acid as a catalyst in an aqueous solution. The effects of MMT and GA contents used on the biodegradability, physical properties, thermal properties and mechanical properties of MC nanocomposites, and crosslinked films were investigated, respectively.

2. Experimental

2.1. Materials

Methyl Cellulose (MC), Tylose H 6000 YP2, was purchased from SE Tylose GmbH & Co., KG, Germany whereas Polargel HV powder, trade name of Montmorillonite (MMT), was supplied by VOLCLAY International Co., Ltd. Glutaraldehyde (GA) solution (25 wt%, molecular weight = 100.11, Bp = 106 °C) under trade name of UNILAB was obtained from Ajex Finechem, New Zealand.

2.2. Preparation of nanocomposite films

2.2.1. Preparation of Montmorillonite suspension

The condition for preparation of MMT suspension by using a homogenizer (IKA T25 basic) was preliminarily investigated. The suitable preparation condition to ensure a completely exfoliated suspension was applied for the preparation of MMT suspension. The performed condition was Polargel HV suspension at 5 wt% and pre-swelling times of 8 days using a homogenizer at a constant mixing speed of 13,500 rpm for 5 min at ambient temperature.

2.2.2. Preparation of Methyl Cellulose nanocomposite films MC/MMT nanocomposite films were prepared by mixing appropriate MMT suspensions obtained from Section 2.2.1 with aqueous MC solutions (2 wt%) by solution intercalation technique over the gelation temperature of MC (50–55 °C). In this study, mixing temperature was about 80 °C. A homogenizer was used for high shear mixing at 13,500 rpm for 5 min. The weight ratio of MC/MMT was varied as 100:0, 100:1, 100:2, 100:3, 100:5, and 100:10. About 30 ml of the obtained MC/MMT solution was poured onto a polystyrene mold. Dried films were obtained after the solvent was evaporated in an air-circulated chamber at ambient temperature. The thickness of the yielded nanocomposite films was in the range of 70–80 μm.

2.3. Preparation of crosslinked Methyl Cellulose films

Aqueous MC solutions (2 wt%) were prepared by dissolving MC powders in water and mixed for 1 min at 80 °C using a homogenizer with a speed of 13,500 rpm. GA and hydrochloric acid were added after the MC solution was cooled to room temperature. The investigated GA contents were varied at 0.5, 1.5, 3.0, 4.5, 6.0, and 12.0 wt%. In each solution, 2 drops of hydrochloric acid were added to yield a solution of pH 3. After stirring using a magnetic stirrer at 700 rpm for 1 h, the homogeneous mixture of MC and GA was obtained. Finally, the resulting dried films were washed by distilled water for 3 h to neutralize the films. The thickness of crosslinked films was approximately the same as that of the nanocomposite films.

3. Specimen characterizations

3.1. X-ray diffraction (XRD)

Interlayer spacing of MMT in nanocomposites was investigated by XRD technique. Samples were detected by X-ray diffractrometer (Bruker model D8 ADVANCE) with CuK α radiation (1.541 Å). The voltage and the current used were 40 kV and 30 mA, respectively. The measurement was scanned at 2θ in the range of 1.5–30.0°. The scan speed was 5.0 s/step with the step size of 0.01°. The basal spacing of the silicate layers (d) was calculated according to Bragg's equation.

3.2. Transmission electron microscopy (TEM)

A qualitative understanding of the internal structure, spatial distribution of the various phases and direct visualization of defect structure was allowed by TECNAI 20 TWIN at an accelerating voltage of 80 kV. The ultrathin film was sectioned at ambient temperature using a Reichert cryoultramicrotome without staining to obtain the thickness of approximately 90 nm.

3.3. Differential scanning calorimetry (DSC)

The thermal behaviors of the MC samples were investigated by Perkin-Elmer Diamond DSC in nitrogen atmosphere. The sample was placed in a sealed aluminum pan. The first heating scan, which was conducted to eliminate water residual, was carried out at a rate of 20 °C/min from room temperature to 150 °C. The second scan was carried out at a heating rate of 10 °C/min from 30 to 300 °C. Glass transition temperature ($T_{\rm g}$) values were identified by using the temperature of the step transition midpoint in the thermogram.

3.4. Thermogravimetric analysis (TGA)

The thermal stability of nanocomposites and crosslinked MC were investigated by Perkin-Elmer Diamond TG/DTA. The sample mass used was about 15 mg. The first heating scan, which was conducted to eliminate water residual, was carried out at a rate of 20 °C/min from room temperature to 150 °C. The second scan was heated from 40 to 500 °C at a heating rate of 20 °C/min in a nitrogen atmosphere. The nitrogen purging flow rate was 100 ml/min. Weight loss of a sample was measured as a function of temperature.

3.5. Dynamic mechanical analysis (DMA)

Dynamic mechanical properties of nanocomposites and crosslinked MC films were investigated by NETZSCH DMA 242C in the tensile mode at a frequency of 1 Hz. The samples were heated from 30 to 250 °C at a rate of 2 °C/min in nitrogen atmosphere. The films with dimen-

sions of about $5 \times 10 \times 0.1 \text{ mm}^3$ were subjected to sinusoidal deformation with 5 mm amplitude. The storage modulus (G'), loss modulus (G''), and loss tangent $(\tan \delta)$ were determined. The T_g was taken as the maximum point on the loss modulus curve in the temperature sweep tests.

3.6. Tensile testing

The tensile strength, elongation at break, and tensile modulus values of nanocomposites and crosslinked MC films were investigated using a universal testing machine (Instron 5567) with a speed of 5.0 mm/min for a gauge length of 50.0 mm at ambient temperature. Samples were cut by scalpel to $130 \times 10 \text{ mm}^2$ in dimension. The reported values were taken from an average of five measurements.

3.7. Fourier transform infrared spectroscopy (FTIR)

To investigate functional groups and the structure of crosslinked MC films, FTIR technique was used (Perkin-Elmer spectrum GX) at the resolution of 4.0 cm⁻¹, at scan number of 64, and frequency of 4000–400 cm⁻¹. The thickness of the films was prepared in the range of 25–30 μm.

3.8. Moisture absorption

The moisture absorption was determined in the nano-composite and crosslinked MC specimens having the dimension of $50 \times 50 \times 0.07$ mm³. The test specimens were dried at 40 °C for 24 h, then cooled in a desiccator, and immediately weighed as the initial weight. The specimens were placed on the aluminum net inside a plastic box $(300 \times 200 \times 110 \text{ mm}^3)$ at 100% RH for 24 h.

After 24 h, the specimens were then weighed immediately to obtain the final weight. The moisture absorption of the sample was calculated according to the following equation:

Moisture absorption (%) =
$$\frac{(W_f - W_i)}{W_i} \times 100$$
 (1)

where W_i and W_f are the weight of composite MC films before and after absorbing moisture.

3.9. Degree of biodegradation

The controlled composite testing of ASTM D5988–96 was modified to find out the degree of biodegradability of nanocomposite and crosslinked films as a function of time. Quantitative tests were performed in an air-tight vessel during a period of 6 weeks. First, 100 g of mixture soil (topsoil: composted manure = 70:30) was added in a 900 ml vessel. Then, 5 g of the tested specimens were placed in the form of fragments and mixed thoroughly with 100 g of the mixture soil. After that, distilled water was added to bring the moisture content to 80–100%. Keep the vessel and lid (with the necessary amount of stopcock grease) in a dark cabinet at ambient temperature. The amount of

CO₂ produced was determined every week using gas chromatography (GC-8A), equipped with a thermal conductivity detector (TCD) and 2 m stainless column packed with Porapak Q (80/100 mesh). The temperatures of the injection port, the column and the detector were maintained at 50 °C. Helium was used as a carrier gas at a flow rate of 25 ml/min. The volume of injected biogas was 0.5 ml.

The area of CO_2 peak, representing CO_2 concentration, was reported. The test method is based on the determination of the net CO_2 evolution, the main product of the biodegradation reaction evolved from the mixture compost minus the CO_2 evolved from the unamended compost (blank).

4. Results and discussion

4.1. Characterization of MC/MMT nanocomposites

4.1.1. Morphology of nanocomposite films

The state of intercalation and exfoliation of nanoparticles has typically been investigated using X-ray diffraction (XRD) analysis. When the interlayer basal spacing increases relative to the original MMT, it is called intercalation. In case that the basal interlayer of the MMT is completely disrupted, it is called exfoliation (Xia, Yih, D'Souza, & Hu, 2003). In addition, transmission electron micrographic (TEM) observation is often used to support XRD results on the nanocomposite morphology.

Fig. 1 shows XRD patterns of MMT powder and MC/5 phr MMT nanocomposite films based on non pre-swelled MMT and pre-swelled MMT, in the region of $2\theta = 1.5$ – 10° . The characteristic peak of MMT powder, a sharp peak, was observed at $2\theta = 6.7^{\circ}$. This value corresponds to the interlayer spacing, d(001) = 1.3 nm, which is similar to a previous report (Park, Liang, Mohanty, Misra, & Drzal, 2004). In the case of MC/5 phr MMT nanocompos-

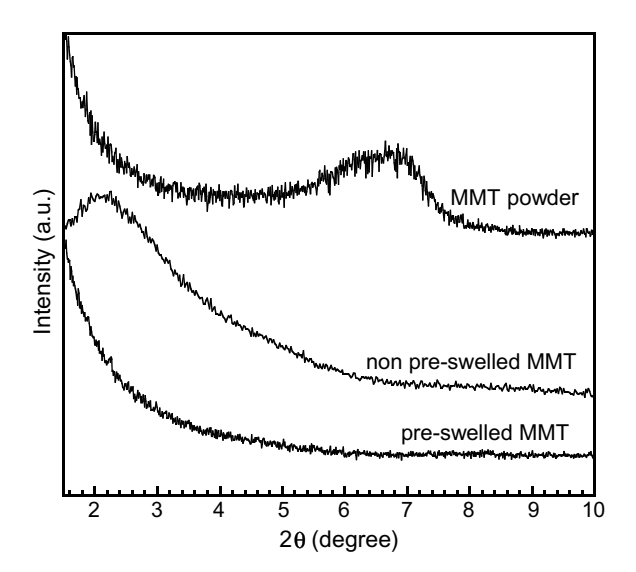


Fig. 1. XRD patterns of MMT powder and MC/5 phr MMT nanocomposite films at various MMT preparations.

ite films using non pre-swelled MMT, a peak was observed at $2\theta = 2.2^{\circ}$ which corresponded to the interlayer spacing, d(001) = 4.3 nm. The angle of the characteristic peak was shifted to the smaller value than that of the MMT powder. This indicates that the molecules of MMT were able to intercalate into the layered silicate of MMT, expanding the basal spacing of the MMT. Therefore, an intercalated structure (within 1.3-4.3 nm) was observed. In the case of MC/5 phr MMT nanocomposite films prepared from preswelled MMT, there were no peaks observed in the diffraction pattern. The phenomenon implied MMT layers in the composites were disordered, thus nanocomposite tended to exhibit exfoliated structure. The proper pre-swelling condition therefore has a positive effect to promote the dispersion of the MMT layers resulting in a highly exfoliated nanocomposite.

XRD patterns of the pure MC, MMT powder, and MC/ MMT nanocomposite films at various MMT contents in the 2θ region of 0.5–30° are shown in Fig. 2. The diffraction intensities were divided by a factor of 100 relative to the nanocomposite intensities in order to place them on the same plot for comparison. The nanocomposite diffraction intensities were vertically overlaid for clarity of presentation. The diffraction pattern of MMT powder had three characteristic peaks with one broad peak at $2\theta = 6.7^{\circ}$ (d = 1.3 nm), which indicated the spacing between the silicate layers and two narrow peaks at $2\theta = 19.8^{\circ}$ and 21.9° . There was no evidence of an MMT basal spacing peak at 1.3 nm in all nanocomposites. The lack of intergallery in MMT diffraction was due to the complete exfoliation and random distribution of the MMT platelets within the MC matrix, which suggests relatively high miscibility of MMT filler and MC matrix. It can be concluded from the XRD study that the nanocomposite containing 1–10 phr of MMT exhibited an exfoliated morphology. However the presence of order at higher d-spacing (>5.8 nm or $2\theta = 1.5^{\circ}$) could not be confirmed from the XRD data in

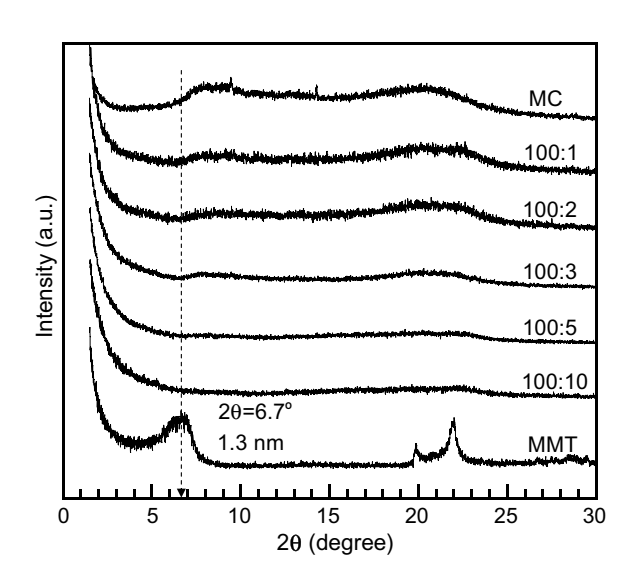


Fig. 2. XRD patterns of pure MC, MMT and MC/MMT nanocomposite films at various contents of MMT.

this study. Further investigation with TEM was, therefore, performed.

For the pure MC film, some broad diffraction peaks were observed between $2\theta=9$ – 21° , indicating some order intermolecular structures of this polymer. For nanocomposite, the area under these peaks indicates the crystallinity of the MC matrix, gradually decreased with increasing the MMT content up to 10 phr. This is probably related to the changes of crystalline morphology for semi-crystalline MC possibly owing to heterogeneous nucleation of MMT particles, which might lower or destroy the crystal perfection or crystallinity of the matrix. The addition of MMT even at the content as low as 1 phr into some polymeric matrices such as Nylon 66 was reported to considerably decrease the crystallinity of the matrix by about 10% (Shen, Phang, Chen, Liu, & Zeng, 2004).

TEM analysis can be used to support XRD results by visualizing MMT dispersion on nanoscale. Nanometer-range intercalated MMT tactoids are shown in Fig. 3a. Dark lines correspond to the cross-section of a MMT sheet ca. 1 nm thick and the gap between two adjacent lines is the interlayer spacing or gallery of the MMT. The measured interlayer spacings between adjacent clay layers of interca-

а

lated tactoids obtained from TEM are consistent with the XRD data.

Fig. 3b and c show TEM micrographs of MC/MMT nanocomposite films at various MMT contents of 5 and 10 phr, respectively. Nanocomposites of MC and MMT clearly reveal disordered platelets of MMT layers in the MC matrix. Dark lines correspond to the cross-section of MMT sheets possibly due to some ionic interaction among the MMT layers. The gap between two adjacent lines was the interlayer spacing or gallery. TEM images of the MC/MMT nanocomposite system with 5 and 10 phr of MMT confirm a well dispersion of MMT layered silicate in the MC matrix with some degree of agglomeration of the MMT layers.

In summary, the results of XRD patterns seen in Fig. 2 suggested that the MMT layers were disordered in the MC matrix. This result was confirmed by TEM images. However, the formations of MMT layers in communities were found in the images. Therefore, the direct visual information of the morphology provides information on the phase distribution and exfoliation behavior with some degree of agglomeration of the MMT, which is similar to a previous work reported by Wibowo et al. (2006).

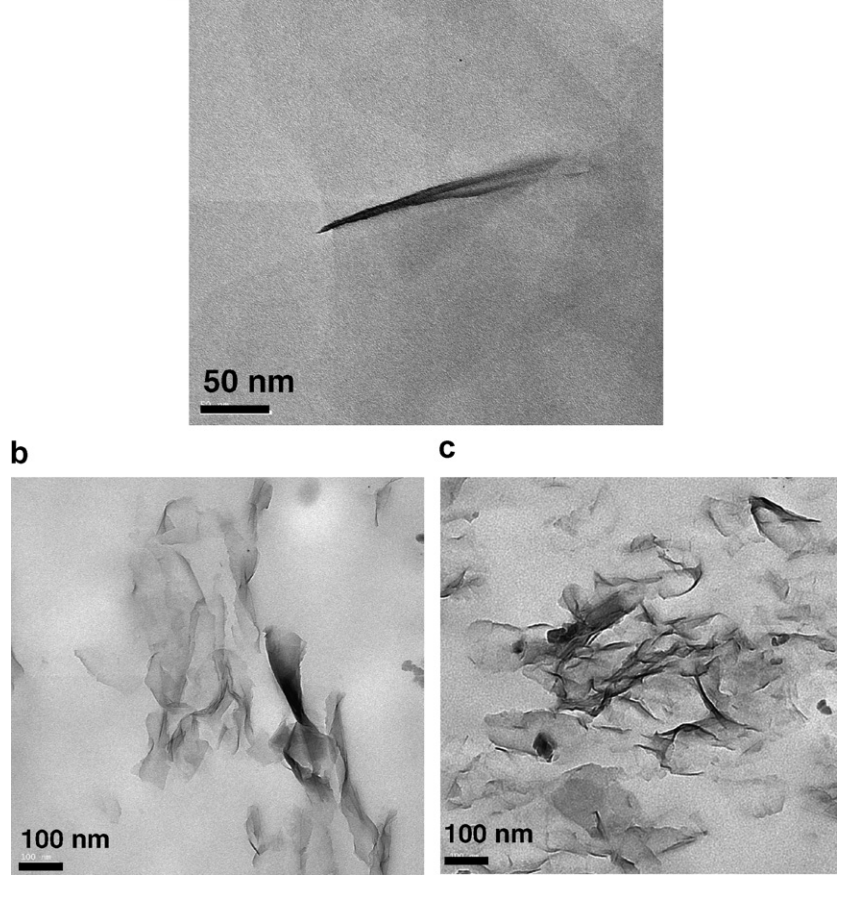


Fig. 3. (a) TEM micrographs of MMT powder at 62,000× magnifications. (b) TEM micrographs of MC/5 phr MMT nanocomposite at 19,000× magnifications. (c) TEM micrographs of MC/10 phr MMT nanocomposite at 19,000× magnifications.

4.1.2. Thermal properties of nanocomposite films

The thermal degradation of the pure MC and MC/ MMT nanocomposites as a function of MMT content is presented in Fig. 4. It can be noticed that a slight weight loss (\sim 1–3 wt%) of MC and MC nanocomposites started below 100 °C. The possible causes for the initial weight loss are probably due to moisture and high water-retention capacity of MC, which is similar to a reported work on hydroxypropylmethylcellulose (HPMC) systems (Park & Ruckenstein, 2001; Sannino et al., 2005). The major weight decrease of pure MC and its nanocomposites took place in the temperature range of 330–400 °C because of the structure degradation of MC. It can be noticed that the thermal decomposition of nanocomposite shifted slightly toward higher temperature from that of the pure MC, which confirmed the enhanced thermal stability due to a barrier effect of the layered MMT on the confined polymers. Beyond 400 °C, all curves were consistent as mainly inorganic residue remained. Like other nanocomposites in the determination of the residual weight, a small amount of MMT also increased the residual weight of MC/MMT because of its inorganic nature. The residual weight of these specimens at 500 °C increased in the order of pure MC < MC/ MMT01 < MC/MMT02 < MC/MMT03 < MC/MMT05 < MC/MMT10 (here number indicates phr of MMT). The improved thermal degradation properties were also observed in the system of chitosan/MMT (Darder, Colilla, & Ruiz-Hitzky, 2003). The authors reported that the addition of MMT enhanced the performance of the char formed, by acting as a superior insulator and mass transports barrier to the volatile products generated during decomposition. It could be explained that the MMT acts as a heat barrier, which enhances the overall thermal stability of the system, and occasionally assists the char formation after thermal decomposition. However, this heat

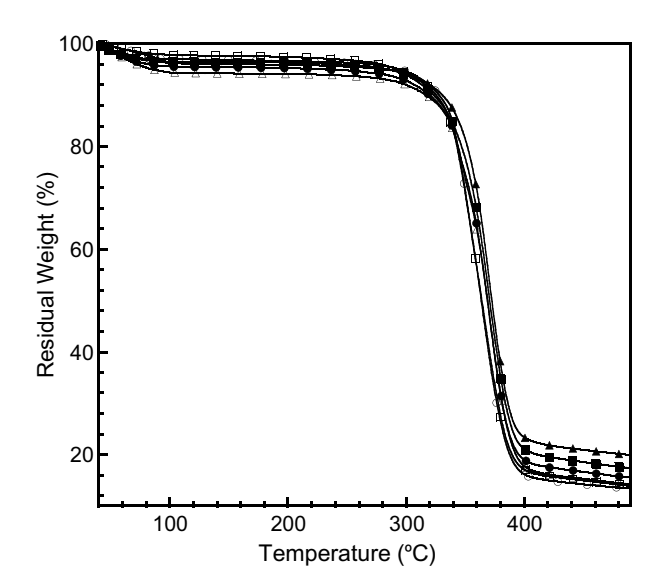


Fig. 4. TGA thermograms of pure MC and MC/MMT nanocomposite films at various contents of MMT: (\bigcirc) pure MC, (\square) 100:1, (Δ) 100:2, (\bullet) 100:3, (\bullet) 100:5, (Δ) 100:10.

barrier effect would sometimes result in a reverse thermal stability. In this case, the stacked silicate layers could hold accumulated heat that could be used as a heat source to accelerate the decomposition process, in conjunction with the heat flow supplied by the outside heat source. This thermal degradation acceleration had been discussed by Sinha and Bousmina (2005).

The DSC thermograms showing glass transition temperature $(T_{\rm o})$ of pure MC and MC/MMT nanocomposites films at various MMT contents are presented in Fig. 5. $T_{\rm g}$ values were taken as the midpoint temperature of the change in specific heat in the transition region. MC curve exhibited T_g at 176 °C, which is similar to T_g of hydroxypropylmethylcellulose (HPMC) (Zaccaron, Oliveira, Guiotoku, Pires, & Soldi, 2005). The $T_{\rm g}$ of the MC nanocomposites slightly shifted to 182 °C with increasing the content of MMT to 10 phr. Theoretically, an increase in T_g was attributed to the restricted thermal motion of polymer in the vicinity of the silicate layers. The slight change of $T_{\rm g}$ was possibly due to the highly rigid anhydroglucose unit of MC. In this type of molecule, the rigidity of the sugar backbone was not changed in a major way by nanoreinforcement, even though there exists a strong bonding between the hydroxyl groups of the anhydroglucose units of MC with the hydroxyl groups on the surfaces and the edges of the exfoliated clay particles (Park et al., 2004).

4.1.3. Dynamic mechanical analysis of nanocomposite films Fig. 6 shows the storage modulus (*G'*) of MC/MMT nanocomposite films in the range of 30–250 °C at various MMT contents. *G'* of the nanocomposite at 10 phr of MMT was higher than that of pure MC and nanocomposite with 1 phr of MMT content for all testing temperatures. In comparison with pure MC at 30 °C, the storage modulus

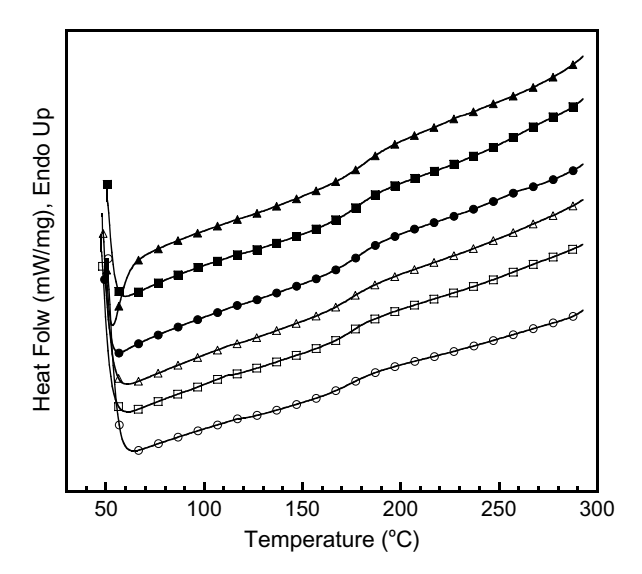


Fig. 5. DSC thermograms showing glass transition temperature of pure MC and MC/MMT nanocomposite films at various contents of MMT: (\bigcirc) pure MC, (\square) 100:1, (Δ) 100:2, (\blacksquare) 100:3, (\blacksquare) 100:5, (\triangle) 100:10.

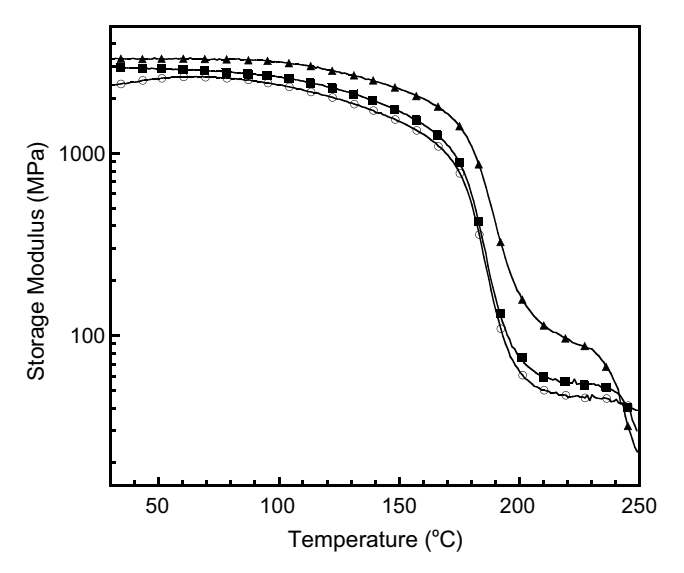


Fig. 6. Storage modulus of MC/MMT nanocomposite films at various contents of MMT: (○) pure MC, (■) 100:1, (▲) 100:10.

of 10 phr nanocomposite increased from 2.4 GPa of pure MC to 3.3 GPa. For all samples, the transition regions from glassy state to rubbery state were in the range of 170–200 °C. Additionally, the improvement of storage modulus was obviously found in the rubbery plateau. This phenomenon can be caused from mechanical reinforcement by the silicate layers (Sinha & Okamoto, 2003).

Fig. 7 indicates mechanical loss tangent $(\tan \delta)$ of the MC and MC/MMT nanocomposite as a function of temperature. The relaxation peaks of the pure MC curve could be observed at 190 °C. That corresponds to the glass transition temperature of the MC, which is similar to the reported $T_{\rm g}$ of same polymer (Park, Park, & Ruckenstein, 2001). The $\tan \delta$ curve for the MC nanocomposites shows the slight shift of the relaxation peaks to higher tempera-

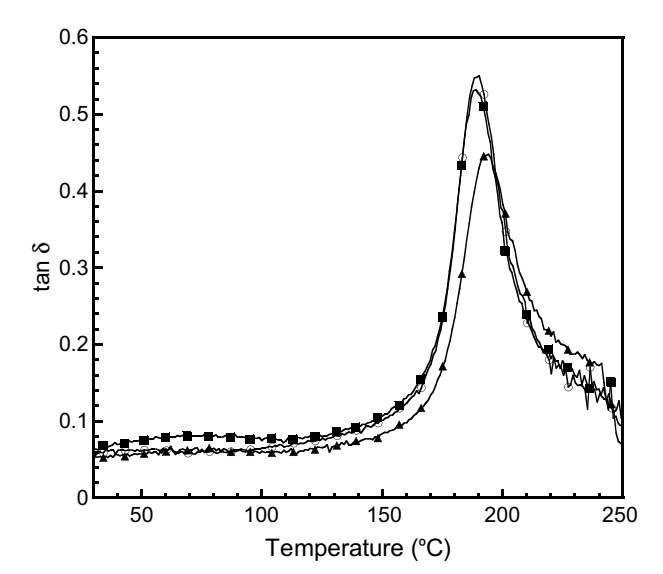


Fig. 7. $\tan \delta$ of MC/MMT nanocomposite films at various contents of MMT: (\bigcirc) pure MC, (\blacksquare) 100:1, (\triangle) 100:10.

ture with increasing MMT content. The $T_{\rm g}$ value was 194 °C for the nanocomposite at 10 phr of MMT. This behavior indicates that the silicate layers in the polymer hybrids have an influence on the mobility of MC chains. This behavior has been described to restricted segmental motions at the organic–inorganic interface neighborhood of intercalated nanocomposites.

4.1.4. Tensile properties of nanocomposite films

Fig. 8 shows the changes of the tensile modulus values at various MMT contents. The tensile modulus of the nanocomposite can be improved by about 65% from 2.0 GPa for pure MC to 3.3 GPa for the nanocomposites contained only 10 phr of MMT. The enhancement of the modulus can be directly attributed to the reinforcement provided by the exfoliation of MMT in the MC. This affected polymer can be thought of as the region of the polymer matrix that is physisorbed on the silicate surface, and is thus stiffened through its affinity for adhesion to the filler surfaces (Shia, Hui, Burnside, & Giannelis, 1998). It is well known that, high aspect ratio fillers as silicate layers and its high surface area exposed to the polymer play a key role in an increase in the modulus with very low filler content. In some cases, the modulus of nanocomposite could be raised about 300% higher than that of the bulk matrix at only 4 wt% of the MMT (Strawhecker & Manias, 2000).

The tensile strength and the elongation at break of MC/MMT nanocomposite films at various MMT contents are shown in Fig. 9. A considerable improvement in tensile strength with a slight decrease in elongation at break was observed with increasing MMT content. The tensile strength was found to increase from 68 MPa for pure MC to 92 MPa for the 10 phr nanocomposites, whereas the elongation at break was slightly reduced from 22.5% of the MC to 18.9% for the 10 phr nanocomposite. This behavior is mainly due to reinforcing effect of MMT from

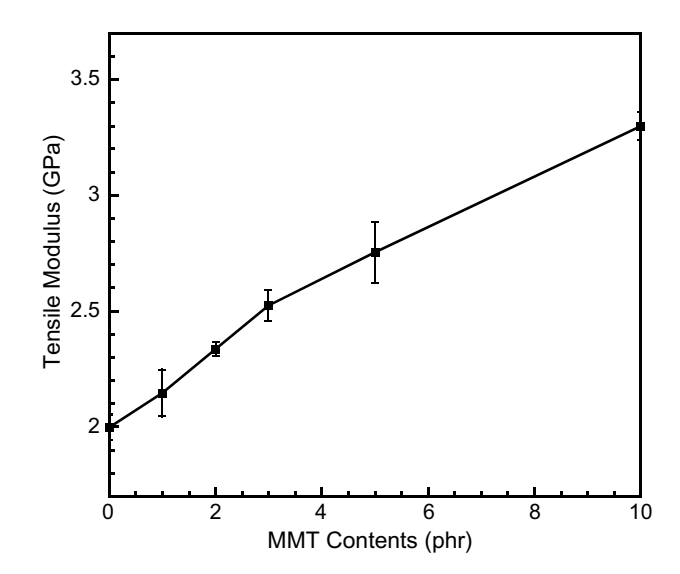


Fig. 8. Tensile modulus of MC/MMT nanocomposite films at various contents of MMT.

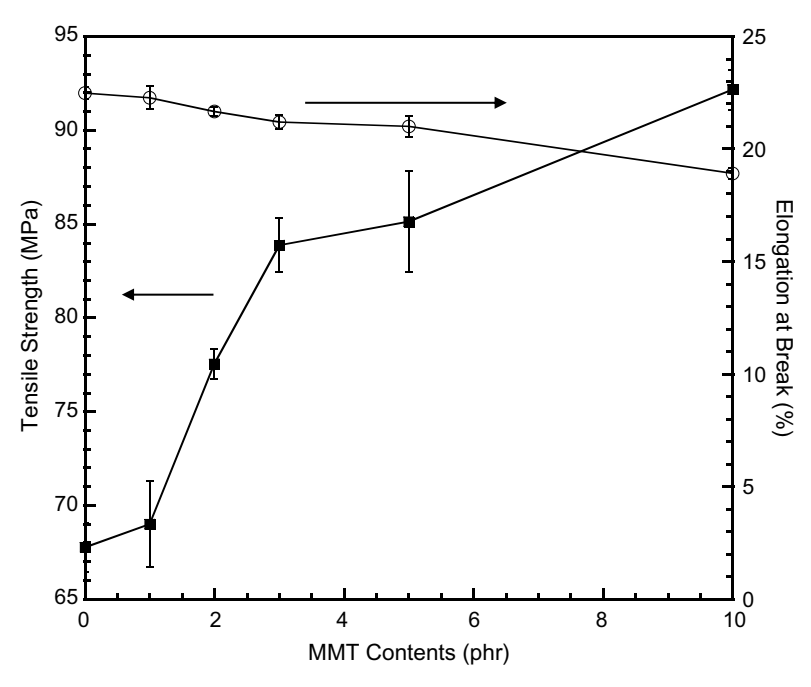


Fig. 9. Tensile strength and elongation at break of MC/MMT nanocomposite films at various contents of MMT: (■) tensile strength, (○) elongation at break.

its high aspect ratio and its enormous surface area discussed above, which leads to high strength improvement.

4.1.5. Moisture absorption of nanocomposite films

Fig. 10 shows a moisture absorption study of pure MC and the MC nanocomposites. The nanocomposites exhibited not only superior mechanical properties but also enhanced moisture resistance. The moisture absorption of nanocomposite films decreased systematically with MMT loading. The MC/MMT nanocomposite films possess lower moisture absorption than that of pure MC, i.e. from

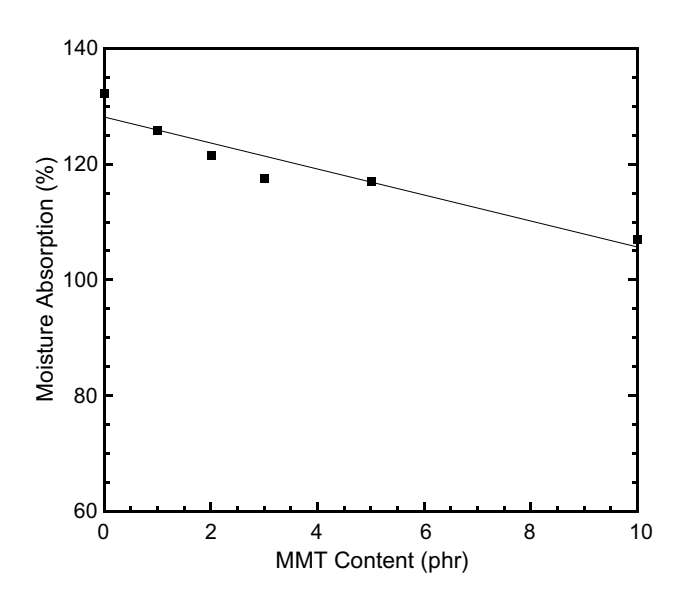


Fig. 10. Moisture absorption of MC/MMT nanocomposite films at various contents of MMT.

133% of pure MC compared to 108% for the 10 phr nanocomposite. This phenomenon can be explained by the fact that MMT layers inherit outstanding mass barrier properties because of the formation of a tortuous path in the presence of layered silicates, which can hinder water diffusion through the nanocomposite specimens. The decrease of moisture absorption in this system is in good agreement with the phenomenon observed in the cassava starch/chitosan/MMT nanocomposite systems (Kampeerapappun et al., 2007) or the system of pullulan–starch nanocomposites (Kristo & Biliaderis, 2007).

4.2. Characterization of crosslinked MC

4.2.1. FTIR spectroscopy investigation of the crosslinked reaction

The FTIR spectra for pure MC and crosslinked films at various amounts of GA crosslinker are shown in Fig. 11. Pure MC had absorption bands related to O—H stretching at 3447 cm⁻¹, C—H stretching at 2837 cm⁻¹, C—O carbonyl stretching from the glucose of the cellulose at 1643 cm⁻¹, C—O stretching from asymmetric oxygen bridge at 1163 cm⁻¹, and ring stretching at 896 cm⁻¹. These values were consistent with those reported by Wang, Yang, Wang, Wang, and Yang (2004). For crosslinked MC, the peaks at 1710 cm⁻¹ (C=O stretching from aldehyde group of GA) is used to indicate the crosslinking reaction. With an increase in the GA over 6.0 wt% in the crosslinked MC, the peak at 1710 cm⁻¹ (C=O from the aldehyde group) substantially increases. The optimal GA content was thus below 6.0 wt%. The appearance of the absorption spectrum also suggested the formation of inter-

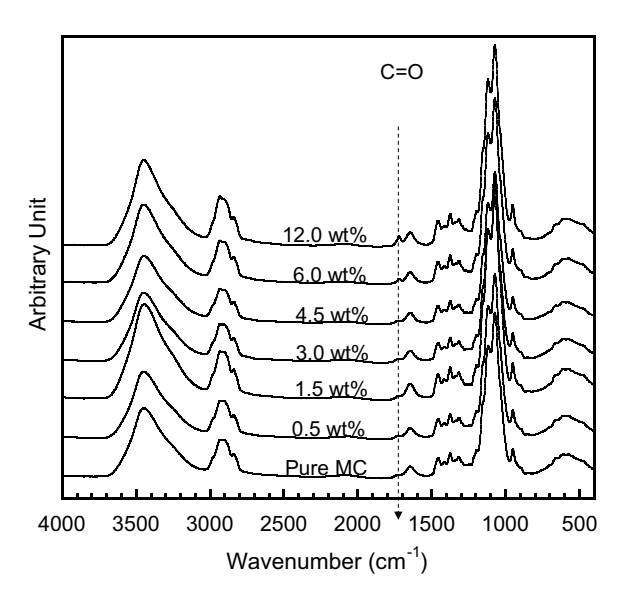


Fig. 11. FTIR spectra of pure MC and MC crosslinked films at various contents of glutaraldehyde.

molecular hydrogen bonding, similar to the results reported for chitosan crosslinked with GA (Kurita, Koyama, & Tanigychi, 1986).

4.2.2. Moisture absorption of crosslinked MC

The effect of the crosslinking agent (GA) contents on moisture absorption ability of crosslinked MC is presented in Fig. 12. All crosslinked MC films in the GA contents range from 0.5 to 12.0 wt% were insoluble in water. When the GA contents increased, moisture absorption also systematically decreased from 133% of uncrosslinked MC to 96% of the crosslinked MC. It can be explained that as the crosslinking of MC increased, the number of hydroxyl

groups of MC decreased. Then, the interaction between hydrogen bonds and water molecules reduced. Moreover, the crosslinking made the polymer chains difficult to move. As a result, the moisture absorption decreased with increasing GA contents. This phenomenon was similar to the work on chitosan crosslinked with tripolyphosphate and genipin at pH 7.4 reported by Mi, Sung, Shyu, Su, and Peng (2003). They stated that the moisture absorption decreased with increasing degrees of crosslinking.

4.2.3. Tensile properties of crosslinked MC

Tensile modulus, tensile strength, and elongation at break were also determined for crosslinked MC with varying concentration of GA crosslinker. The testing conditions are the same as those used for nanocomposite films evaluation.

Fig. 13 illustrates a relationship between tensile modulus of crosslinked MC films at various contents of GA. Comparing with uncrosslinked MC film, the tensile modulus of crosslinked MC film at 4.5 wt% of GA improved by 45% (from 2.0 to 2.9 GPa). From 6.0 to 12.0 wt% of GA, this value slightly decreased. This phenomenon can be explained that GA led to network structures, which decreased the mobility of the polymer chains. Therefore, the crosslinked materials were rigid. When the GA content was in excess, i.e. higher than 4.5 wt% in this case, it might function as a plasticizer that softened the crosslinked films.

The tensile strength and the elongation at break at various contents of GA are shown in Fig. 14. The increase of GA content had no significant effect on the tensile strength, while the elongation at break decreases with increasing the GA content. The elongation at break of crosslinked MC was decreased about 87% for the GA contents of 12 wt% because the excess amount of the crosslinking agent started to act as a plasticizer.

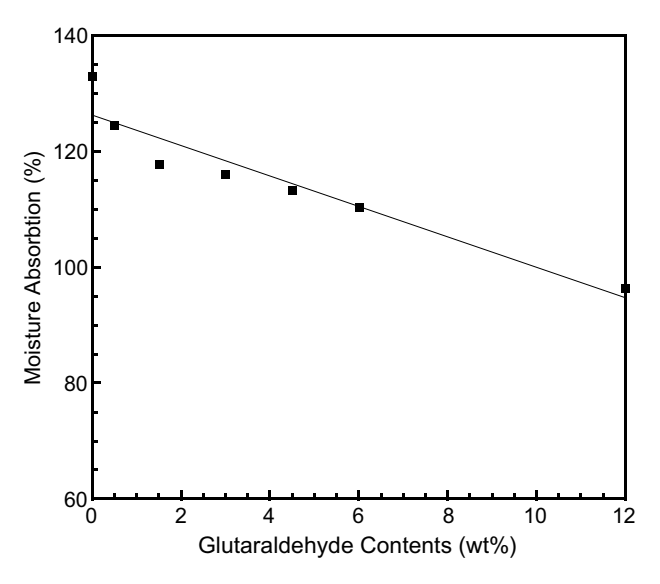


Fig. 12. Moisture absorption of MC crosslinked films at various contents of glutaraldehyde.

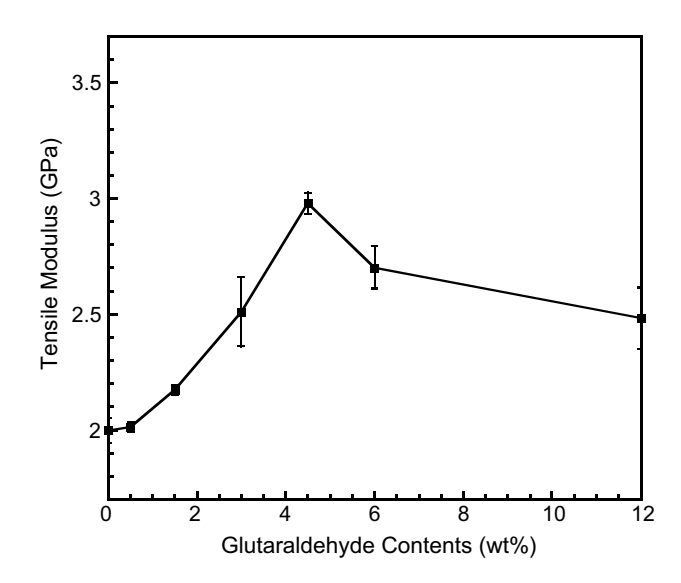


Fig. 13. Tensile modulus of MC crosslinked films at various contents of glutaraldehyde.

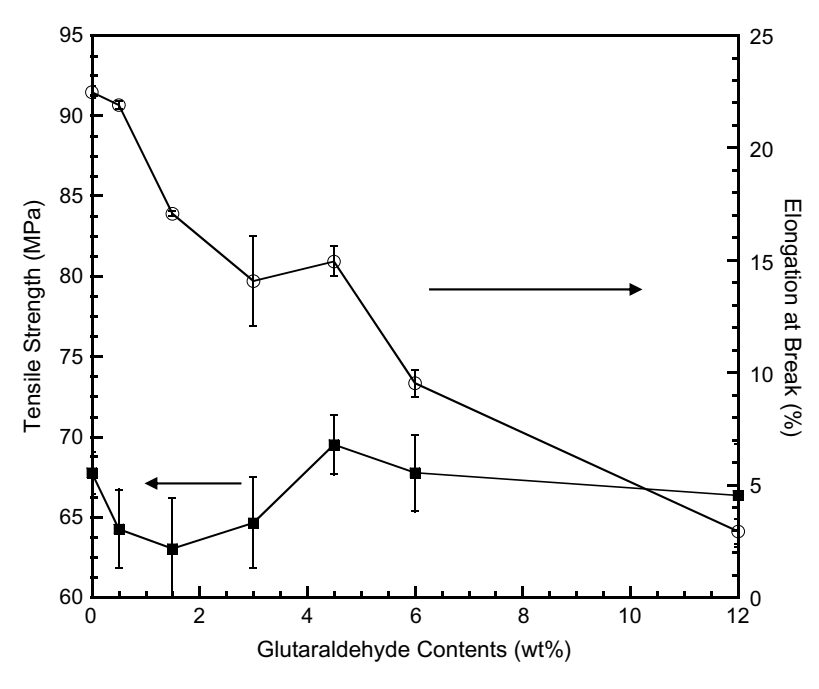


Fig. 14. Tensile strength and elongation at break of MC crosslinked films at various contents of glutaraldehyde: (■) tensile strength, (○) elongation at break.

4.2.4. Dynamic mechanical analysis of crosslinked MC

For all GA concentration of the crosslinked films, significant enhancement of storage modulus (G') can be seen in the investigated temperature ranges as presented in Fig. 15. At 250 °C (temperature in the rubbery plateau region) the addition of GA increases plateau modulus of the crosslinked films which relates to an increase in degree of crosslinking in the specimen. The crosslinked MC film at 4.5 wt% of GA showed the highest crosslinking density. The higher degree of crosslinking led to denser network structures, which decreased the mobility of the polymer

chains. Therefore, the higher crosslinked materials have more rigidity in nature. When the contents of GA were 6 wt% (i.e. excess level), the crosslink density became lower than its highest plateau, i.e. at 4.5 wt% GA. This was because GA acted as a plasticizer that softened the crosslinked films.

Fig. 16 presents the DMA thermograms of MC cross-linked films and pure MC as mechanical loss tangent ($\tan \delta$) against temperature. The relaxation peak corresponded to the $T_{\rm g}$ of the pure MC can be observed at 190 °C. The $\tan \delta$

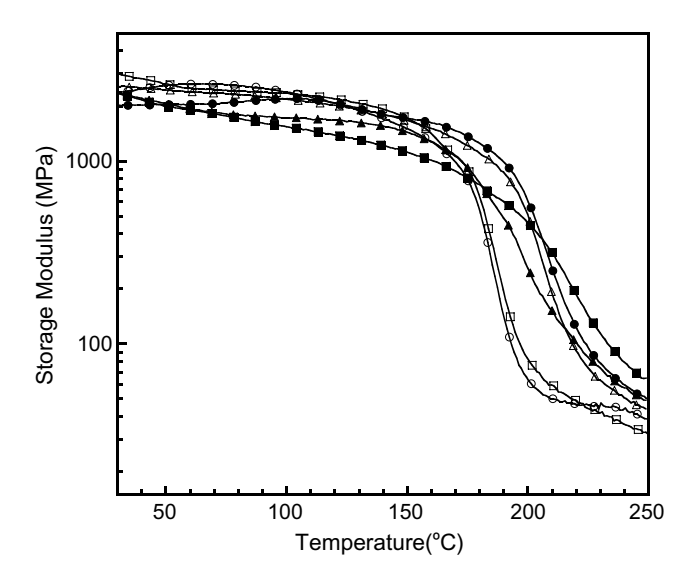


Fig. 15. Storage modulus of pure MC and MC crosslinked films at various contents of glutaraldehyde: (\bigcirc) pure MC, (\square) 0.5 wt%, (\triangle) 1.5 wt%, (\blacksquare) 3.0 wt%, (\blacksquare) 4.5 wt%, (\triangle) 6.0 wt%.

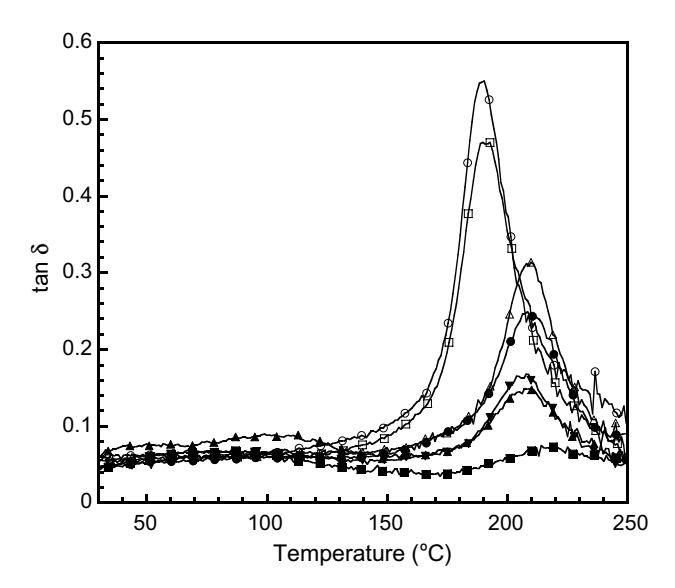


Fig. 16. $\tan \delta$ of pure MC and MC crosslinked films at various contents of glutaraldehyde: (\bigcirc) pure MC, (\square) 0.5 wt%, (Δ) 1.5 wt%, (\bullet) 3.0 wt%, (\bullet) 4.5 wt%, (\bullet) 6.0 wt%, (\bullet) 12.0 wt%.

curves for the MC crosslinked films show the shift of the relaxation peaks to higher temperature with increasing the GA from 0.5 to 4.5 wt%. That means the film with 4.5 wt% of GA rendered the highest $T_{\rm g}$ (219 °C). When the amount of GA was greater than 4.5 wt%, the $T_{\rm g}$ decreased due to the plasticizing effect as mentioned earlier. Generally, the height of $\tan \delta$ exhibits the ratio between viscous and elastic behaviors. In this figure, $\tan \delta$ peak of pure MC is highest. It can be observed that the height of the curves decreased with an addition of the GA crosslinker. At 4.5 wt% of GA which is about the optimal GA quantity, the films showed the highest elastic behavior from the highest network density thus showing the small $\tan \delta$ peak.

4.3. Biodegradability of MC/MMT nanocomposite and crosslinked MC films

The quantitative study of net CO_2 evolution from pure MC film, nanocomposite films and crosslinked films during 6 weeks is shown in Fig. 17. When comparing the results of nanocomposite films and crosslinked films, the amount of CO_2 from crosslinked films < nanocomposite films < pure MC film. That means the crosslink formation could have a greater effect on prolonging biodegradation of MC films than the addition of MMT.

The decrease of biodegradability of MC/MMT nanocomposites was possibly caused from the interaction and adhesion of MC and layered silicate surfaces of MMT, which restricted segmental motion at the interface. A part of MC chains was hidden by the silicate layers on the surface of the film, which forced the degraders to diffuse into the bulk of the film through more tortuous paths. Therefore, the effective path length and time for the diffusion

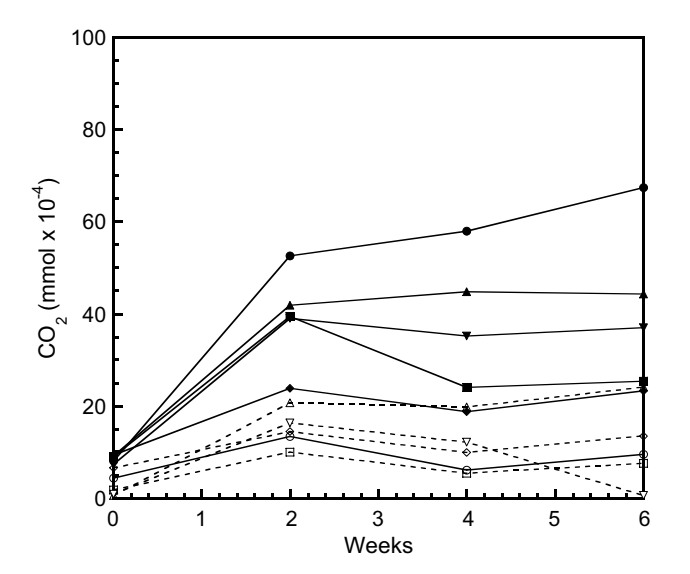


Fig. 17. Net CO₂ evolution of pure MC and MC/MMT nanocomposite films: (\bullet) pure MC, (\bullet) 100:1, (\bullet) 100:3, (\bullet) 100:5, (\blacktriangledown) 100:10, and MC crosslinked films at various contents of glutaraldehyde: (\bigcirc) 0.5 wt%, (\square) 1.5 wt%, (\triangle) 3.0 wt%, (\lozenge) 4.5 wt%, (\square) 6.0 wt%.

of degraders were increased, and the biodegradation of MC was hindered (Lee et al., 2002).

The decreased permeability may also be related to the decrease of the biodegradability. The hydrolysis of MC matrix was likely to depend on transporting water from the surface into the bulk of the film. The water permeability of MC crosslinked films was reduced with increasing amount of GA. Therefore, the biodegradability of crosslinked MC decreased with increasing amount of crosslinking agent (Weian, Wei, & Yue, 2005).

Although both MMT and GA could delay the biodegradation of MC films, the crosslinking could have a greater effect to hinder erosion process and biodegradation process than the addition of nanoparticles.

5. Conclusions

MC-based biodegradable polymer prepared by solution intercalation was achieved. The MC/MMT nanocomposites prepared by MMT suspension was exfoliated nanocomposite confirmed by XRD and TEM results. Both $T_{\rm g}$ and $T_{\rm d}$ of MC/MMT nanocomposite were slightly increased with MMT content (1–10 phr). The $T_{\rm g}$ of nanocomposite increased with MMT contents from 190 °C (pure MC film) to 194 °C (at 10 phr of MMT), whereas tensile strength and Young's modulus of the nanocomposites were improved notably with increasing the MMT loadings. When compared with pure MC film, the elongation at break slightly decreased about 16%. This phenomenon is attributed to the high aspect ratio and enormous surface area of MMT during exfoliation. In addition, moisture absorption of nanocomposite was reduced about 19%.

From the FTIR spectra of crosslinked MC films, it can be noticed that there was a peak presenting excess aldehyde at the GA contents of 6.0 wt%. This peak was not found at the concentration of at most 4.5 wt%. The crosslinking increased $T_{\rm g}$ with GA content from 190 °C (pure MC film) to 219 °C (at 4.5 wt% of GA). In addition, the crosslinking slightly improved the tensile properties. When comparing between pure MC film and the film at 4.5 wt% of GA, the modulus was increased about 45% due to network structures caused by GA. The elongation at break remarkably decreased about 34%. In addition, moisture absorption of crosslinked film was reduced about 27%.

In the biodegradation test, the biodegradability of MC-based biodegradable polymers can be retarded by both crosslinking and nanocomposite techniques. In comparison, the crosslinking technique had more potential to hinder the biodegradation process. The main reason is that the crosslinkage could prevent water to diffuse through the bulk.

In summary, both MC-based biodegradable polymers in the forms of nanocomposites and crosslinked polymers were found to improve biodegradation properties. The MC/MMT nanocomposites could significantly improve tensile properties. For MC crosslinked film, biodegradable and thermal properties were outstandingly enhanced when compared with MC/MMT nanocomposites.

Acknowledgements

The authors would like to acknowledge the National Nanotechnology Center (Nanotec.), Thailand, for the financial support. One of the authors, S.R., would like to thank the Hitachi Scholarship Foundation, Japan, for the fellowship to perform part of this work in Japan. Prof. Toemsak Srikhirin, Faculty of Science, Mahidol University, Thailand, is also gratefully acknowledged for the TEM experiment.

References

- Aminabhavi, T. M., Balundgi, R. H., & Cassidy, P. E. (1990). A review on biodegradable plastics. *Polymer-Plastics Technology and Engineering*, 29, 235–262.
- Avella, M., Vlieger, J. J., Errico, M. E., Fischer, S., Vacca, P., & Volpe, M. G. (2005). Biodegradable starch/clay nanocomposite films for food packaging applications. *Food Chemistry*, 93, 467–474.
- Coma, V., Sebti, I., Pardon, P., Pichavant, F. H., & Deschamps, A. (2003). Film properties from crosslinking of cellulosic derivatives with a polyfunctional carboxylic acid. *Carbohydrate Polymers*, 51, 265–271.
- Crosby, N. T. (1981). Food packaging material. Aspects of analysis and migration of contaminates. London: Applied Science Publisher Ltd.
- Darder, M., Colilla, M., & Ruiz-Hitzky, E. (2003). Biopolymer-clay nanocomposites based on chitosan intercalated in montmorillonite. *Chemistry of Materials*, 15, 3774–3780.
- Doi, Y. (1990). *Microbial polyesters*. New York: VCH Publishers, Inc. Gupta, B., & Revagade, N. (2007). Poly(lactic acid) fiber: An overview.
- Progress in Polymer Science, 32, 455–482.
- Kampeerapappun, P., Aht-Ong, D., Pentrakoon, D., & Srikulkit, K. (2007). Preparation of cassava starch/montmorillonite composite film. *Carbohydrate Polymers*, 67, 155–163.
- Krikorian, V., & Pochan, D. J. (2003). Poly (L-lactic acid)/layered silicate nanocomposite: Fabrication, characterization, and properties. *Chemistry of Materials*, 15, 4317–4324.
- Kristo, E., & Biliaderis, C. G. (2007). Physical properties of starch nanocrystal-reinforced pullulan films. Carbohydrate Polymers, 68, 146–158.
- Kurita, K., Koyama, Y., & Tanigychi, A. (1986). Studies on chitin. IX. Crosslinking of water-soluble chitin and evaluation of the products as adsorbents for cupric ion. *Journal of Applied Polmer Science*, 30, 1169–1176.
- Lee, S. R., Park, H. M., Lim, H. L., Kang, T., Li, X., & Cho, W. J. (2002). Microstructure, tensile properties, and biodegradability of aliphatic polyester/clay nanocomposites. *Polymer*, 43, 2495–2500.
- Li, H. Y., Chen, Y. F., & Xie, Y. S. (2004). Nanocomposites of crosslinking polyanhydrides and hydroxyapatite needles: Mechanical and degradable properties. *Materials Letters*, 58, 281.
- Mangiacapra, P., Gorrasi, G., Sorrentino, A., & Vittoria, V. (2005). Biodegradable nanocomposites obtained by ball milling of pectin and montmorillonites. *Carbohydrate Polymers*, 64, 516–523.
- Marras, S. I., Zuburtikudis, I., & Panayiotou, C. (2007). Nanostructure vs. microstructure: Morphological and thermomechanical characterization of poly(L-lactic acid)/layered silicate hybrids. *European Polymer Journal*, 43, 2191–2206.

- Mi, F. L., Sung, H. W., Shyu, S. S., Su, C. C., & Peng, C. K. (2003).
 Synthesis and characterization of biodegradable TPP/genipin co-crosslinked chitosan gel beads. *Polymer*, 44, 6521–6530.
- Park, H. M., Liang, X., Mohanty, A. K., Misra, M., & Drzal, L. T. (2004). Effect of compatibilizer on nanostructure of the biodegradable cellulose acetate/organoclay nanocomposites. *Macromolecules*, 37, 9076–9082.
- Park, J. S., & Ruckenstein, E. (2001). Viscoelastic properties of plasticized methylcellulose and chemically crosslinked methylcellulose. *Carbohy-drate Polymers*, 46, 373–381.
- Park, J. S., Park, J. W., & Ruckenstein, E. (2001). Thermal and dynamic mechanical analysis of PVA/MC blend hydrogels. *Polymer*, 42, 4271–4280.
- Sannino, A., Pappada, S., Madaghiele, M., Maffezzoli, A., Ambrosio, L., & Nicolais, L. (2005). Crosslinking of cellulose derivatives and hyaluronic acid with water-soluble carbodiimide. *Polymer*, 46, 11206–11212.
- Shen, L., Phang, I. Y., Chen, L., Liu, T., & Zeng, K. (2004). Nanoindentation and morphological studies on nylon 66 nanocomposites. I. Effect of clay loading. *Polymer*, 45, 3341–3349.
- Shia, D., Hui, C. Y., Burnside, S. D., & Giannelis, E. P. (1998). An interface model for the prediction of Young's modulus of layered silicate–elastomer nanocomposites. *Polymer Composites*, 19, 608–615.
- Sinha, R. S., & Okamoto, M. (2003). Polymer/layered silicate nanocomposites: A review from preparation to processing. *Progress in Polymer Science*, 28, 641–1539.
- Sinha, R. S., & Bousmina, M. (2005). Biodegradable polymers and their layered silicate nanocomposites: In greening the 21st century materials world. *Progress in Material. Science*, 50, 962–1079.
- Strawhecker, K. E., & Manias, E. (2000). Structure and properties of poly(vinyl alcohol)/Na+montmorillonite nanocomposites. *Chemistry Letters*, 12, 2943–2949.
- Wach, R. A., Mitomo, H., Nagasawa, N., & Yoshii, F. (2003). Radiation crosslinking of methylcellulose and hydroxyethylcellulose in concentrated aqueous solutions. Nuclear Instruments & Methods in Physics Research Section B-Beam Interactions with Materials and Atoms, 211, 533–544.
- Wang, S., Song, C., Chena, G., Guoa, T., Liub, J., Zhang, B., et al. (2005). Characteristics and biodegradation properties of poly(3-hydroxybutyrate-co-3-hydroxyvalerate)/organophilic montmorillonite (PHBV/OMMT) nanocom-posite. *Polymer Degradation and Stability*, 87, 69–76.
- Wang, X. L., Yang, K. K., Wang, Y. Z., Wang, D. Y., & Yang, Z. (2004). Crystallization and morphology of a novel biodegradable polymer system: Poly(1,4-dioxan-2-one)/starch blends. *Acta Materialia*, 52, 4899–4905.
- Weian, Z., Wei, L., & Yue, F. (2005). Synthesis and properties of a novel hydrogel nanocomposites. *Material Letters*, 59, 2876–2880.
- Wibowo, A. C., Manjusri, M., Hwan, M. P., Lawrence, T. D., Richard, S., & Amar, K. M. (2006). Biodegradable nanocomposites from cellulose from cellulose acetate: Mechanical, morphological, and thermal properties. *Composites Part A-Applied Science and Manufacturing*, 37, 1428–1433.
- Xia, X., Yih, S., D'Souza, N. A., & Hu, Z. (2003). Swelling and mechanical behavior of poly(N-isopropylacrylamide)/namontmorillonite layered silicates composite gels. Polymer, 44, 3389–3393.
- Yang, J. H., Yu, J. G., Feng, Y., & Ma, X. F. (2006). Study on the properties of ethylenebisformamide plasticized corn starch (EPTPS) with various original water contents of corn starch. *Carbohydrate Polymers*, 69, 256–261.
- Zaccaron, C. M., Oliveira, R., Guiotoku, M., Pires, A., & Soldi, A. (2005). Blends of hydroxypropyl methylcellulose and poly(1-vinylpyrrolidone-co-vinyl acetate): Miscibility and thermal stability. *Polymer Degradation and Stability*, 90, 21–27.